Optimization of Weld Parameters in Wire and Arc-Based Directed Energy Deposition of High Strength Low Alloy Steels

Van Thao Le[1,*], Dinh Si Mai[1], Van Thuc Dang[1], Duc Manh Dinh[1], Thi Hong Cao[2], Van Anh Nguyen[3]

[1]Advanced Technology Center, Le Quy Don Technical University, Hanoi, Vietnam

[2]Institute for Tropical Technology, Vietnam Academy of Science and Technology, Hanoi, Vietnam

[3]Welding Engineering and Laser Processing Centre, Cranfield University, Bedford, UK

Received 10 August 2022; received in revised form 27 September 2022; accepted 30 September 2022

DOI: https://doi.org/10.46604/aiti.2022.10658

Abstract

This paper aims to investigate the fabrication of high strength low alloy (HSLA) steels by wire and arc-based directed energy deposition (WADED). Firstly, the relationship between the process variables (including the travel speed-V, the current-C, and the voltage-U) and the geometrical characteristics of weld beads (including the bead height (BH), bead width (BW), and melting pool length (MPL)) was investigated. Secondly, the optimal process variables were identified using the desirability approach. The results indicate that voltage-U has the highest impact on BW and MPL, meanwhile the travel speed-V is the most impacting factor on BH. The optimal variables for the WADED process of HSAL steels are V = 0.3 m/min, C = 160 A, and U = 19 V. The component fabricated with the optimal variables is fully dense without spatters and defects, confirming the efficiency of the WADED process for HSLA steels.

Keywords: WADED, HSLA steel, weld bead, optimal variables

1. Introduction

Emerged since the 1980s, additive manufacturing (AM) technologies, especially metallic AM, are strongly developed, and they are becoming the key technology in the Industry 4.0 era [1]. Because of the layer-by-layer manufacturing principle, AM technologies can fabricate very complex structures from various materials, including metallic alloys that are very difficult to machine by conventional processes such as milling and turning [2]. The metallic AM technologies can be categorized based on the energy source and feedstock form or the fabrication methods. According to the feedstock form and the fabrication methods, there are two main groups of metallic AM, i.e., powder bed fusion (PBF) and directed energy deposition (DED) [3].

Compared to PBF-AM processes, DED-AM can produce metallic components with larger dimensions and can be applied effectively for repairing and remanufacturing applications [4-7]. The DED-AM processes include two technologies: (i) laser and powder-based DED (LPDED) using a laser source to melt metal powder (Fig. 1(a)), and (ii) wire and arc-based DED (WADED) utilizing an arc source to melt the metal wire (Fig. 1(b)). The nozzle in the WADED is a welding torch, and the wire feeding method depends on the used welding source, for example, gas tungsten arc welding (GTAW), plasma arc welding (PAW), and gas metal arc welding (GMAW) [8]. Compared to other metal AM technologies, WADED has a superior rate of material deposition (from 3 to 8 kg/h), high efficiency of material utilization, low costs of investing systems and devices, and easy implementation [9].

* Corresponding author. E-mail address: vtle@lqdtu.edu.vn

The metal wire available in the welding market can be used for WADED processes. They are also much cheaper than metal powder used in PBF-AM and LPDED. Therefore, WADED is becoming a potential solution for manufacturing components with large and wide dimensions [10].

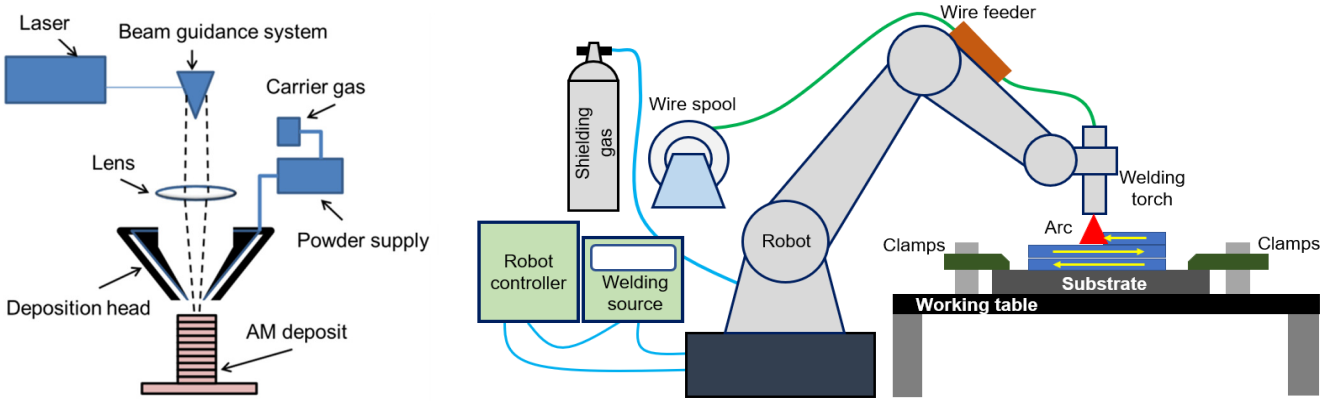

(a) The LPDED process [11] (b) The WADED process

Fig. 1 Schemas of LPDED and WADED processes

Among metals used in WADED, including steels, aluminum, titanium, and nickel-based alloys, steels are the most investigated materials because of their relatively low costs, wide applications, and availability in the welding market. In the literature, many steel grades have been investigated and fabricated with the WADED processes, for example, low-carbon steels (e.g., ER70S-6) [12-14], austenite stainless steels (e.g., 304, 308L, 308LSi, 309L, and 316L) [15], and high- strength low alloy (HSLA) steels (e.g., ER110S-G and ER120S-G) [16-18]. The HSLA steels are largely utilized for manufacturing lightweight structures and high strength components in many sectors, for example, automotive, shipbuilding, tools and die industries. These steel grades have high strength, toughness, weldability, and low costs [19].

Recently, many researchers have investigated and fabricated components from HSLA steels by the WADED processes. Sun et al. [20] produced thin-wall HSLA steel components by WADED and examined the anisotropy in mechanical characteristics. They stated that the strengths of the as-fabricated component in the horizontal direction were lower than those in the vertical direction. Rodrigues et al. [16] studied the impact of the heat input on the microstructures and mechanical properties of the WADEDed thin-wall HSLA steel part. They observed that there were no significant differences in microstructure between the specimens fabricated with low and high levels of heat input. Dirisu et al. [19] analyzed the toughness properties of HSLA steels produced by WADED. They found that the refinement in grains and the increase in density of grain boundaries resulted in high resistance to failure of the samples in the vertical direction. Fang et al. [21] also fabricated HSLA steel parts by WADED. The researcher observed that the part had a superior balance in strength and ductility. The variation in microhardness was due to the difference of thermal histories in different regions of the component.

Although certain authors have investigated HSLA steels fabricated by the WADED processes, as mentioned above, they mainly analyzed microstructures and mechanical characterization of the as-built material, as well as the influence of process variables on the quality of the part. Until now, the studies on predicting and optimizing process variables in WADED of HSLA steel to obtain the expected geometrical properties of weld beads are still limited. Most of the previously mentioned studies have selected the process variables (e.g., the arc voltage, welding current, and wire-feed speed) based on the suggestion of the wire manufacturers for conventional welding or based on several tests, while the WADED process is very different from welding. In WADED processes, the quality and geometry of weld beads (e.g., stable and smooth shape and less spatter) notably affect the process stability and the appearance of as-fabricated components [22-25]. Therefore, this study aims to explore the relationship between the process variables {C, U, and V} and the geometrical characteristics of weld beads {BW, BH, and MPL} and identify optimal process parameters that produce weld beads with expected geometrical properties.

2. Materials and Methods

2.1. Materials and the WADED system

In this investigation, the HSLA steel wire (SM-110) with a 1.2-mm diameter supplied by Hyundai Welding and the low-carbon steel substrates with a size of 200 × 200 × 10 mm had been utilized. The chemical elements of the wire are 1.95%Ni, 1.90%Mo, 0.34%Cr, 0.58%Mo, 0.80%Si, 0.089%C, 0.010%P, 0.004%S, and %Fe in balance (wt.%). A WADED system (Fig. 2(a)) consists of a GMAW source, a welding torch, a welding wire feeder, a 6-axis robot, and a shielding gas feeder was used to fabricate the samples (e.g., single weld tracks, Fig. 2(b) and Fig. 2(c)). The relationships between the wire feed speed and welding current in this GMAW-AM system is approximately increasing linearly. A mixed gas of argon (80%) and CO_2 (20%) with 16 L/min in flow speed was applied during the WADED process.

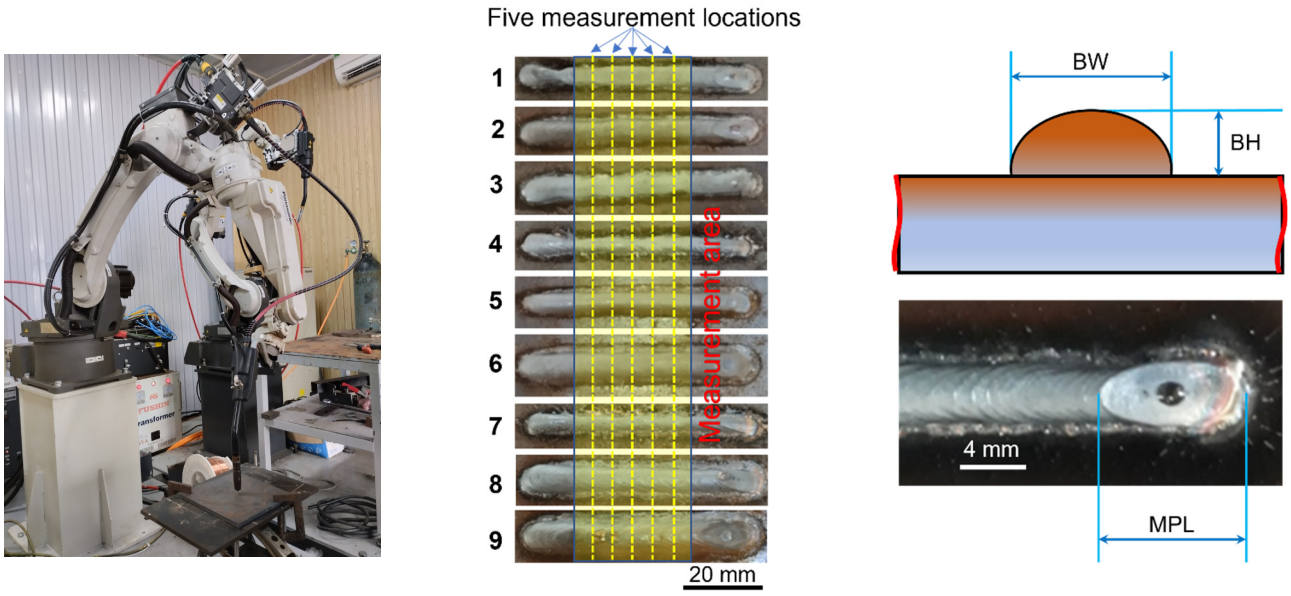

(a) The welding robot (b) Weld bead samples (c) WB's characteristics

Fig. 2 The WADED system, the WB samples with the measurement area, and the response description

2.2. Experimental procedure

To achieve the goal of the study, the research procedure shown in Fig. 3 was performed. The research procedure includes the following steps: (i) identification of the process variables and their ranges, (ii) design of experiment, (iii) fabrication of single weld beads by the WADED process, (iv) measurement of the responses (i.e., BH, BW, and MPL), development of regression models for the responses and determining the impact of process variables on the responses through the analysis of variance (ANOVA), and (v) the optimization of process variables.

To observe the relationship between the process variables and the responses, the Taguchi L9 orthogonal array was adopted to design the experimental plan. Three input variables, including the current-C, the travel speed of the weld torch-V, and the voltage-U were selected for the investigation because they directly influence the shape and dimensions of the weld beads. Three levels for each variable were used (Table 1). As a result, there were nine experiment runs.

Table 1 Input variables and their levels for the DoE

Item	Levels		
Voltage-U (V)	18	20	22
Current-C (A)	120	140	160
Travel speed-V (m/min)	0.3	0.4	0.5

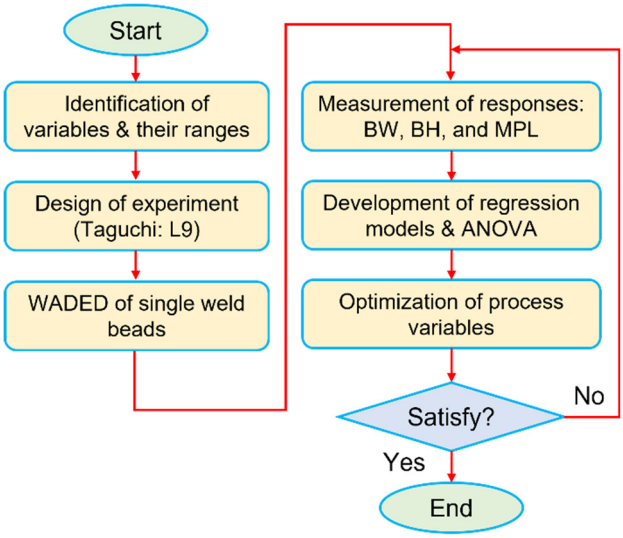

Fig. 3 The study flowchart

After the fabrication of weld bead samples, the responses of weld beads, including BH, BW, and MPL were measured. These characteristics of weld beads play important roles in the WADED process. BH and BW are related to the layer width and height, whereas the MPL is related to the planning of deposition paths. The measurements were executed in the stable regions of welding beads (Fig. 2(b)) utilizing a digital Mitutoyo caliper with 0.01 mm in resolution and ± 0.02 mm in accuracy. The BW and BH were measured five times at five locations in the middle zone of weld beads (Fig. 2(b)). Finally, the average value of the five measurements of BW and BH was taken for analysis. On the other hand, the measurement of MPL was repeated three times to ensure the reliability of the measurement results. The experiment runs and measured results were presented in Table 2.

Table 2 Experiment runs and the response measurement

Experiment run	Input variables			Responses		
	Current-C (A)	Voltage-U (V)	Travel speed-V (m/min)	BW (mm)	BH (mm)	MPL (mm)
1	120	18	0.3	5.39	3.09	11.26
2	120	20	0.4	5.86	2.54	11.64
3	120	22	0.5	5.82	1.82	12.39
4	140	18	0.4	4.58	2.92	10.49
5	140	20	0.5	5.41	2.33	11.34
6	140	22	0.3	7.51	2.81	13.52
7	160	18	0.5	4.18	2.77	9.79
8	160	20	0.3	6.87	3.00	11.95
9	160	22	0.4	7.82	2.37	13.24

2.3. *Analysis and optimization methods*

To evaluate the impact of input variables on the responses and identify the impact contribution of each input, the ANOVA and the Minitab software was adopted. The ANOVA was executed with a 5% significance level and a 95% confidence level. In the WADED, BH, and BW are expected to be maximal while the MPL is minimal to enhance productivity. As a result, the optimization problem was formulated as Eq. (1).

$$\begin{cases} Find\ \{C,\ U,\ V\} \\ To\ maximize\ \{BH,\ BW\}\ and\ minimize\ \{MPL\} \\ Subject\ to\ \{120 \le C \le 160\ A,\ 18 \le U \le 22\ V,\ 0.3 \le V \le 0.5\ m/min\} \end{cases} \quad (1)$$

The optimal input variables were estimated by the desirability function (DF) method [26]. Moreover, the weight for each response (i.e., BW, BH, and MPL) was identified by the CRITIC method [27]. The steps of the CRITIC method are described as follows:

Step 1: Construct the decision matrix (DM) of k experimental runs and p evaluation attributes: $\mathrm{DM} = [m_{ij}]_{k\times p}$.

Step 2: Normalize the DM using Eq. (2):

$$\hat{m}_{ij} = \frac{m_{ij} - m_j^{worst}}{m_j^{best} - m_j^{worst}} \tag{2}$$

where $\hat{m}_{ij}$ is the normalized value of the i^{th} alternative for j^{th} attribute, m_j^{best} and m_j^{worst} are the best and worst values of j^{th} attribute.

Step 3: Calculate the standard deviation of each normalized attribute using Eq. (3):

$$\sigma_j = \sqrt{\frac{\sum_{i=1}^{k}(\hat{m}_{ij} - \overline{m}_j)^2}{k}} \tag{3}$$

where k is the number of experimental runs and $\overline{m}_j$ is the average value of j^{th} normalized attribute.

Step 4: Construct the symmetric matrix $[cc_{ij}]_{k\times k}$ with the linear-correlation coefficient cc_{ij} between the attributes. cc_{ij} is calculated by Eq. (4):

$$cc_{ij} = \frac{\sum_{l=1}^{k}(\hat{m}_{li} - \overline{m}_i)(\hat{m}_{lj} - \overline{m}_j)}{\sqrt{\sum_{l=1}^{k}(\hat{m}_{li} - \overline{m}_i)^2 \sum_{l=1}^{k}(\hat{m}_{lj} - \overline{m}_j)^2}} \tag{4}$$

Step 5: Calculate the attribute information AI_j by Eq. (5):

$$AI_j = \sigma_j \sum_{l=1}^{k}(1 - cc_{jl}) \tag{5}$$

Step 6: Calculate the weight w_j for each attribute (i.e., response):

$$w_j = \frac{AI_j}{\sum_{j=1}^{p} AI_j} \tag{6}$$

3. Results and Discussion

3.1. Regression models

The regressive models of the responses BW, BH, and MPL are shown in Tables 3, 4, and 5, respectively. They were developed with the help of Minitab software. In the case of BW, the p-values of U and V in Table 3, are smaller than 0.05, while the p-value of C is bigger than 0.05, meaning that U and V are the significant terms of the BW model. The values of R-sq, R-sq(adj), and R-sq(pred) are 95.67%, 93.07%, and 83.83%, respectively. It indicates that the BW model has acceptable accuracy and can terms be used to predict the response in the entire design space.

For the BH model, all the p-values of C, U, and V in Table 4 are smaller than 0.05. Therefore, all the model terms C, U, and V are significant. The values of the determination coefficients R-sq, R-sq(adj), and R-sq(pred) are 96.51%, 94.72%, and

86.18%, respectively, indicating a reasonable accuracy of the BH model. This model can also be used to predict the response in the entire design space.

For the developed model of MPL, the p-values of U and V in Table 5 are smaller than 0.05, while the p-value of C is bigger than 0.05, indicating that U and V are the significant term of the MPL model. The values of R-sq, R-sq(adj), and R-sq(pred) are 97.73%, 96.36%, and 91.15%, respectively. Therefore, the MPL model has an acceptable accuracy, and it can be used to predict the responses (i.e., BW, BH, and MPL) in the whole design space.

Table 3 ANOVA of BW

Source	DF	Seq SS	Contribution	Adj SS	Adj MS	F-Value	P-Value
Regression	3	11.8791	95.67%	11.8791	3.9597	36.81	0.001
C	1	0.5424	4.37%	0.5424	0.5424	5.04	0.075
U	1	8.1713	65.81%	8.1713	8.1713	75.97	0.000
V	1	3.1654	25.49%	3.1654	3.1654	29.43	0.003
Error	5	0.5378	4.33%	0.5378	0.1076	-	-
Total	8	12.4169	100.00%	-	-	-	-
Regressive model			$BW = -4.93 + 0.01503 \times C + 0.5835 \times U - 7.26 \times V$				
R-sq = 95.67%			R-sq(adj) = 93.07%			R-sq(pred) = 83.83%	

Table 4 ANOVA of BH

Source	DF	Seq SS	Contribution	Adj SS	Adj MS	F-Value	P-Value
Regression	3	1.26082	96.51%	1.26082	0.420272	46.14	0.000
C	1	0.07935	6.07%	0.07935	0.079350	8.71	0.032
U	1	0.52807	40.42%	0.52807	0.528067	57.98	0.001
V	1	0.65340	50.02%	0.65340	0.653400	71.74	0.000
Error	5	0.04554	3.49%	0.04554	0.009108	-	-
Total	8	1.30636	100.00%	-	-	-	-
Regressive model			$BH = 6.109 + 0.00575 \times C - 0.1483 \times U - 3.300 \times V$				
R-sq = 96.51%			R-sq(adj) = 94.42%			R-sq(pred) = 86.18%	

Table 5 ANOVA of MPL

Source	DF	Seq SS	Contribution	Adj SS	Adj MS	F-Value	P-Value
Regression	3	11.3854	97.73%	11.3854	3.79513	71.65	0.000
C	1	0.0160	0.14%	0.0160	0.01602	0.30	0.606
U	1	9.6520	82.85%	9.6520	9.65202	182.22	0.000
V	1	1.7173	14.74%	1.7173	1.71735	32.42	0.002
Error	5	0.2648	2.27%	0.2648	0.05297	-	-
Total	8	11.6502	100.00%	-	-	-	-
Regressive model			$MPL = 1.55 - 0.00258 \times C + 0.6342 \times U - 5.350 \times V$				
R-sq = 97.73%			R-sq(adj) = 96.36%			R-sq(pred) = 91.15%	

3.2. Relationship between the input variables and the responses

As shown in Fig. 4(a), it is indicated that the BW increases when U and C increment. Meanwhile, V shows an opposite impact tendency. The BW decreases with the augmentation in V. Based on the ANOVA results (Table 3), the voltage-U has the most impact contribution to the BW with 65.81%, followed by the travel speed (25.49%), and the current (4.37%), respectively. The influence of the input variables on the BW can be explained as follows. An increase in voltage also makes an increase in the length and spreading of the arc. Therefore, BW becomes larger with a higher level of voltage [28]. An increase in welding current leads to an increase in wire feed speed and material deposition, resulting in an augmentation in melting pool size and in

the width of weld beads (BW) [23]. Oppositely, an increase in travel speed causes a reduction in material deposition quantity per length unit. Therefore, the BW becomes narrow as the travel speed increases [28].

The influence of the input variables on the BH is shown in Fig. 4(b). It is shown that the increase in both the voltage-U and the travel speed-V causes a decrease in the BH. On the other hand, the BH increases when the current-C increase. However, the BH sightly increases when C increases from 140 A to 160 A. In this case, the travel speed-V reveals the highest impact on the BH with a contribution of 50.02%, followed by the voltage-U (40.42%), and the current-C (6.02%), respectively (Table 4). Indeed, when increasing the travel speed, the quantity of deposited materials per length unit is reduced. Hence, BH is reduced [28-29]. The spreading area of the arc is larger when the voltage increases, leading to flatter weld beads [30]. As a result, BH reveals a reducing trend with an increment in voltage. As C increases, the wire feeding speed augments. Hence, the volume of materials deposited increases, leading to an increase in BH [28].

For the MPL, as depicted in Fig. 4(c), it strongly increases when the voltage increases, meanwhile the MPL slightly increases with the increase in the current-C. The MPL, on the other hand, increases as V augments from 0.3 m/min to 0.4 m/min, after that it decreases. These findings can be explained by the ANOVA results (Table 5). It is shown that the voltage-C has the most influential contribution of 82.85% to MPL, while the current has the lowest impact contribution of 0.14% to MPL.

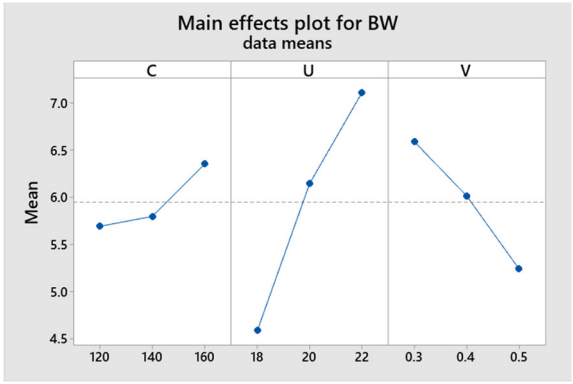

(a) Effects of process variables on BW

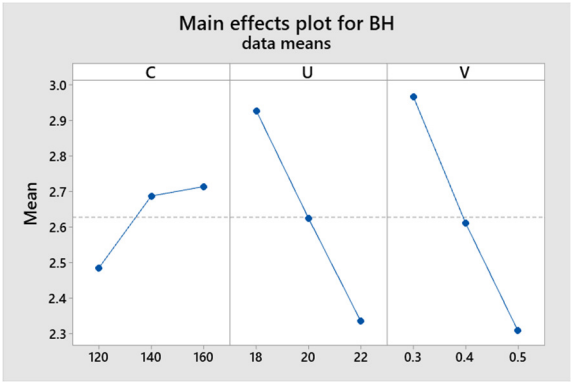

(b) Effects of process variables on BH

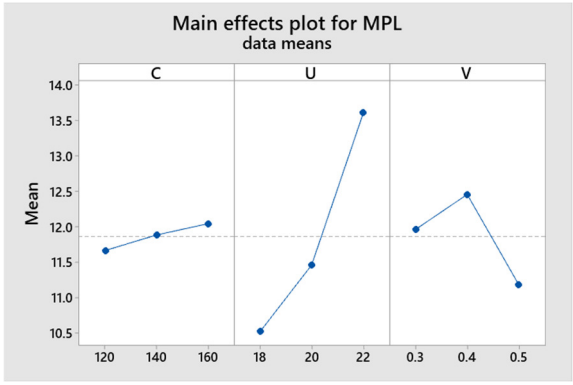

(c) Effects of process variables on MPL

Fig. 4 Influences of the input variables on the responses

3.3. Optimization results

As mentioned previously, the weights for the responses were calculated by the CRITIC method. The weight values of BW, BH, and MPL were 0.42, 0.23, and 0.34, respectively. The solution of the multi-attribute optimization problem (Eq. (1)) was shown in Fig. 5. It indicated that the optimal input variables are {C = 160 A, V = 0.3 m/min, and U = 19 V}. This set of input parameters is corresponding to the DF value of 0.8651 and the predicted responses BW = 6.39 mm, BH = 3.22 mm, and MPL = 11.59 mm. Compared to the worst case, where the BH was the smallest (the experiment run #3), the optimal input parameters allow enhancing the BH and BW by 77% and 10%, respectively, while reducing the MPL by 6%.

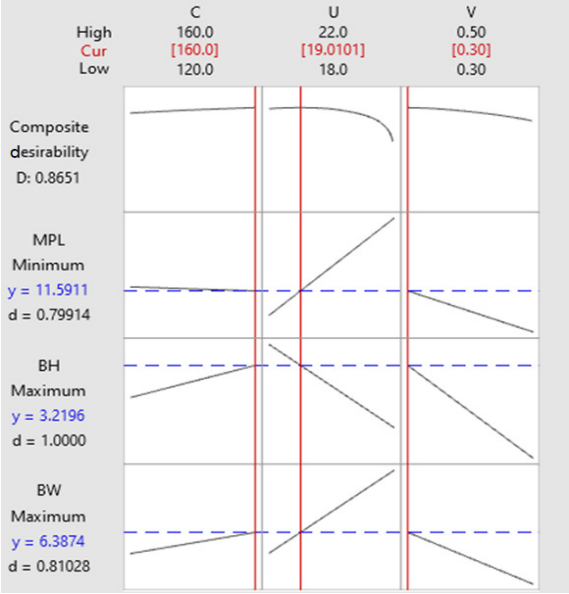

Fig. 5 Optimization solution

To confirm the efficiency of the optimal input parameters, they were tested to fabricate a three-bead multi-layer-cylindric wall (Fig. 6). It is shown that the optimal parameters enable the production of smooth weld beads without spatters and major defects. There is only a minor defect in shape on the top surface at the stopping point of the weld path. In this investigation, as the starting point and the ending point of the weld path were not identical, there was an overlap between the arc-striking and the arc-extinguishing regions of the arc (Fig. 7(a)). Therefore, the difference in height between the arc-striking and the arc-extinguishing regions was compensated. On the other hand, when the starting and the ending points are identical, there is a space in the circle weld bead between the starting and the ending points (Fig. 7(b). As the number of layers increases, the gap depth increases, resulting in major defects in the shape of the part.

Fig. 6 Multi-bead multi-layer cylindric part

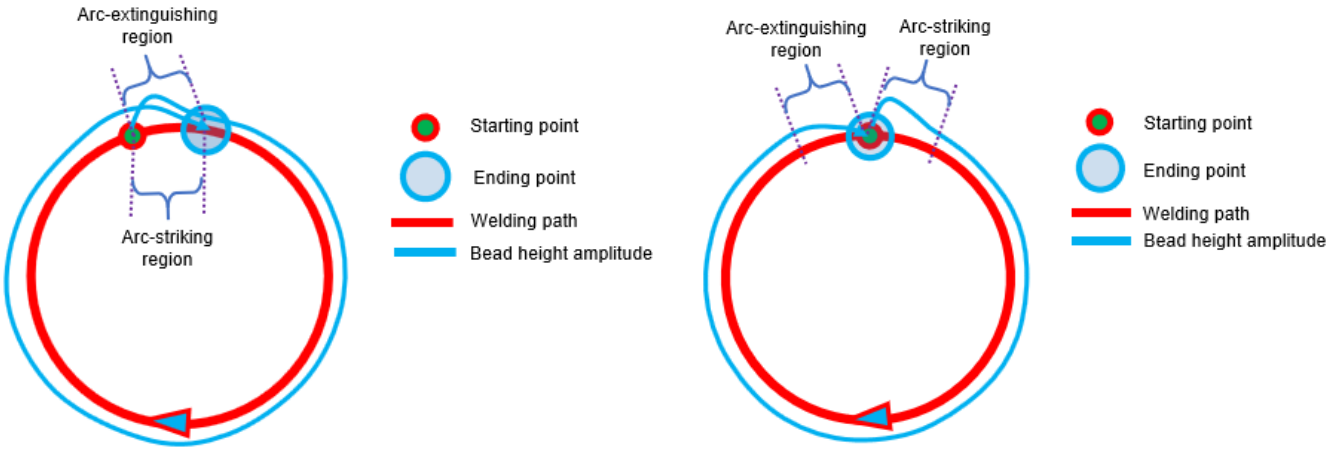

(a) Not identical (b) Identical

Fig. 7 Programming of a circle weld path: the starting point and the ending point

Moreover, the as-built material is fully dense without defects such as pores, cracks, and lack of fusion. The microstructure mainly consists of α-ferrite phases in acicular and granular morphologies (Fig. 8(a)). The EDX analysis results also indicate that the as-built material has similar chemical elements as the wire material (Fig. 8(b)). The melted metal was perfectly protected by the shielding gas during the WADED process.

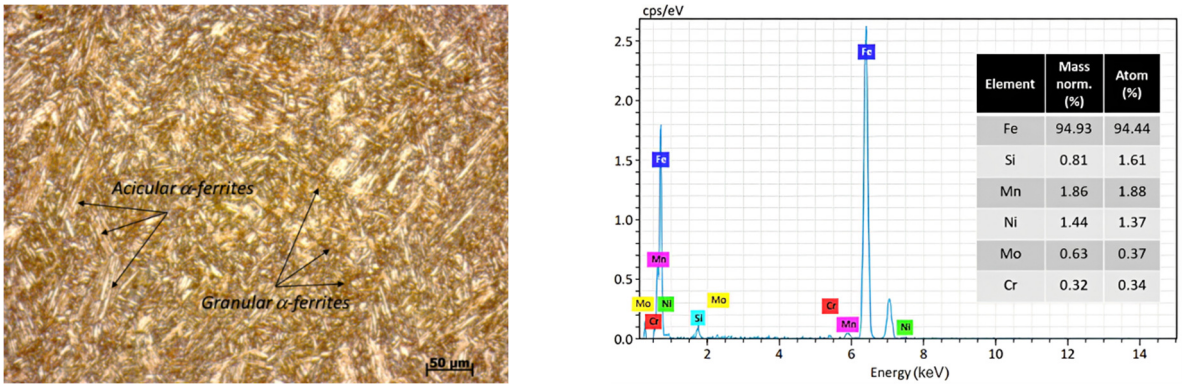

(a) Microstructure (b) Chemical elements

Fig. 8 Microstructure and chemical elements of the as-built material

4. Conclusions

In this study, HSLA steel was utilized as the raw material in the WADED process. The study aims to predict the connection between the main process variables {C, U, and V} and the geometrical characteristics of weld beads {BW, BH, and MPL}. Furthermore, finding the optimal process variables is also the study's aim. The main findings of this investigation are highlighted as follows.

(1) The voltage-U has the highest impact on BW and MPL, meanwhile the travel speed-V is the most impacting factor on BH. An increase in U leads to an increase in BW and MPL and a decrease in BH. On the other hand, an increase in V causes a decrease in both BW and BH.

(2) All the predictive models of BW, BH, and MPL have an acceptable accuracy with the determination values R-sq = 95.67%, 96.51%, and 97.73%, respectively. They can be applied to predict the responses in the entire design space.

(3) The optimal process variables for the WADED process of SM-110 HSLA steel are V = 0.3 m/min, C = 160 A, and U = 19 V. The component fabricated with the optimal variables has a smooth top surface. Moreover, spatters and defects don't present in the fabrication. The as-built material is fully dense without defects such as pores, cracks, and lack of fusion.

(4) The microstructure of the as-built material is mainly composed of ferrite phases with acicular and granular morphologies. Its chemical elements also have the comparable weight percentage to those of the wire material.

Conflicts of Interest

The authors declare no conflict of interest.

Acknowledgment

This investigation is funded by Le Quy Don Technical University under grant number ĐH.03.2022. The authors would like to acknowledge great supports from WeldTech Company for our project.

References

[1] U. M. Dilberoglu, B. Gharehpapagh, U. Yaman, and M. Dolen, "The Role of Additive Manufacturing in the Era of Industry 4.0," Procedia Manufacturing, vol. 11, pp. 545-554, 2017.

[2] S. M. Thompson, L. Bian, N. Shamsaei, and A. Yadollahi, "An Overview of Direct Laser Deposition for Additive Manufacturing; Part I: Transport Phenomena, Modeling and Diagnostics," Additive Manufacturing, vol. 8, pp. 36-62, October 2015.

[3] V. T. Le, H. Paris, and G. Mandil, "The Development of a Strategy for Direct Part Reuse Using Additive and Subtractive Manufacturing Technologies," Additive Manufacturing, vol. 22, pp. 687-699, August 2018.

[4] V. T. Le, H. Paris, and G. Mandil, "Process Planning for Combined Additive and Subtractive Manufacturing Technologies in a Remanufacturing Context," Journal of Manufacturing Systems, vol. 44, no. 1, pp. 243-254, July 2017.

[5] A. Ramalho, T. G. Santos, B. Bevans, Z. Smoqi, P. Rao, and J. P. Oliveira, "Effect of Contaminations on the Acoustic Emissions during Wire and Arc Additive Manufacturing of 316L Stainless Steel," Additive Manufacturing, vol. 51, article no. 102585, March 2022.

[6] S. Li, J. Y. Li, Z. W. Jiang, Y. Cheng, Y. Z. Li, S. Tang, et al., "Controlling the Columnar-to-Equiaxed Transition during Directed Energy Deposition of Inconel 625," Additive Manufacturing, vol. 57, article no. 102958, September 2022.

[7] T. A. Rodrigues, N. Bairrão, F. W. C. Farias, A. Shamsolhodaei, J. Shen, N. Zhou, et al., "Steel-Copper Functionally Graded Material Produced by Twin-Wire and Arc Additive Manufacturing (T-WAAM)," Materials & Design, vol. 213, article no. 110270, January 2022.

[8] V. T. Le, D. S. Mai, M. C. Bui, K. Wasmer, V. A. Nguyen, D. M. Dinh, et al., "Influences of the Process Parameter and Thermal Cycles on the Quality of 308L Stainless Steel Walls Produced by Additive Manufacturing Utilizing an Arc Welding Source," Welding in the World, vol. 66, no. 8, pp. 1565-1580, August 2022.

[9] D. Jafari, T. H. J. Vaneker, and I. Gibson, "Wire and Arc Additive Manufacturing: Opportunities and Challenges to Control the Quality and Accuracy of Manufactured Parts," Materials & Design, vol. 202, article no. 109471, April 2021.

[10] S. W. Williams, F. Martina, A. C. Addison, J. Ding, G. Pardal, and P. Colegrove, "Wire + Arc Additive Manufacturing," Materials Science and Technology, vol. 32, no. 7, pp. 641-647, 2016.

[11] W. E. Frazier, "Metal Additive Manufacturing: A Review," Journal of Materials Engineering and Performance, vol. 23, no. 6, pp. 1917-1928, June 2014.

[12] J. Xiong, Y. Li, R. Li, and Z. Yin, "Influences of Process Parameters on Surface Roughness of Multi-Layer Single-Pass Thin-Walled Parts in GMAW-Based Additive Manufacturing," Journal of Materials Processing Technology, vol. 252, pp. 128-136, February 2018.

[13] V. T. Le, "A Preliminary Study on Gas Metal Arc Welding-Based Additive Manufacturing of Metal Parts," VNUHCM Journal of Science and Technology Development, vol. 23, no. 1, pp. 422-429, February 2020.

[14] V. T. Le, Q. H. Hoang, V. C. Tran, D. S. Mai, D. M. Dinh, and T. K. Doan, "Effects of Welding Current on the Shape and Microstructure Formation of Thin-Walled Low-Carbon Parts Built By Wire Arc Additive Manufacturing," Vietnam Journal of Science and Technology, vol. 58, no. 4, pp. 461-472, July 2020.

[15] W. Jin, C. Zhang, S. Jin, Y. Tian, D. Wellmann, and W. Liu, "Wire Arc Additive Manufacturing of Stainless Steels: A Review," Applied Sciences, vol. 10, no. 5, article no. 1563, March 2020.

[16] T. A. Rodrigues, V. Duarte, J. A. Avila, T. G. Santos, R. M. Miranda, and J. P. Oliveira, "Wire and Arc Additive Manufacturing of HSLA Steel: Effect of Thermal Cycles on Microstructure and Mechanical Properties," Additive Manufacturing, vol. 27, pp. 440-450, May 2019.

[17] J. G. Lopes, C. M. Machado, V. R. Duarte, T. A. Rodrigues, T. G. Santos, and J. P. Oliveira, "Effect of Milling Parameters on HSLA Steel Parts Produced by Wire and Arc Additive Manufacturing (WAAM)," Journal of Manufacturing Processes, vol. 59, pp. 739-749, November 2020.

[18] A. V. Nemani, M. Ghaffari, and A. Nasiri, "Comparison of Microstructural Characteristics and Mechanical Properties of Shipbuilding Steel Plates Fabricated by Conventional Rolling versus Wire Arc Additive Manufacturing," Additive Manufacturing, vol. 32, article no. 101086, March 2020.

[19] P. Dirisu, S. Ganguly, A. Mehmanparast, F. Martina, and S. Williams, "Analysis of Fracture Toughness Properties of Wire + Arc Additive Manufactured High Strength Low Alloy Structural Steel Components," Materials Science and Engineering: A, vol. 765, article no. 138285, September 2019.

[20] L. Sun, F. Jiang, R. Huang, D. Yuan, C. Guo, and J. Wang, "Anisotropic Mechanical Properties and Deformation Behavior of Low-Carbon High-Strength Steel Component Fabricated by Wire and Arc Additive Manufacturing," Materials Science and Engineering: A, vol. 787, article no. 139514, June 2020.

[21] Q. Fang, L. Zhao, B. Liu, C. Chen, Y. Peng, Z. Tian, et al., "Microstructure and Mechanical Properties of 800-MPa-Class High-Strength Low-Alloy Steel Part Fabricated by Wire Arc Additive Manufacturing," Journal of Materials Engineering and Performance, 2022. https://doi.org/10.1007/s11665-022-06784-7

[22] V. T. Le, D. S. Mai, and Q. H. Hoang, "A Study on Wire and Arc Additive Manufacturing of Low-Carbon Steel Components: Process Stability, Microstructural and Mechanical Properties," Journal of the Brazilian Society of Mechanical Sciences and Engineering, vol. 42, no. 9, article no. 480, September 2020.

[23] V. T. Le, D. S. Mai, T. K. Doan, and Q. H. Hoang, "Prediction of Welding Bead Geometry for Wire Arc Additive Manufacturing of SS308l Walls Using Response Surface Methodology," Transport and Communications Science Journal, vol. 71, no. 4, pp. 431-443, May 2020.

[24] Z. Wang, S. Zimmer-Chevret, F. Léonard, and G. Abba, "Prediction of Bead Geometry with Consideration of Interlayer Temperature Effect for CMT-Based Wire-Arc Additive Manufacturing," Welding in the World, vol. 65, no. 12, pp. 2255-2266, December 2021.

[25] J. Xiong, G. Zhang, J. Hu, and L. Wu, "Bead Geometry Prediction for Robotic GMAW-Based Rapid Manufacturing through a Neural Network and a Second-Order Regression Analysis," Journal of Intelligent Manufacturing, vol. 25, no. 1, pp. 157-163, February 2014.

[26] V. C. Nguyen, T. D. Nguyen, and V. T. Le, "Optimization of Sustainable Milling of SKD11 Steel under Minimum Quantity Lubrication," Proceedings of the Institution of Mechanical Engineers, Part E: Journal of Process Mechanical Engineering, 2022. https://doi.org/10.1177/09544089221110978

[27] G. C. M. Patel and Jagadish, "Experimental Modeling and Optimization of Surface Quality and Thrust Forces in Drilling of High-Strength Al 7075 Alloy: CRITIC and Meta-Heuristic Algorithms," Journal of the Brazilian Society of Mechanical Sciences and Engineering, vol. 43, no. 5, article no. 244, May 2021.

[28] D. T. Sarathchandra, M. J. Davidson, and G. Visvanathan, "Parameters Effect on SS304 Beads Deposited by Wire Arc Additive Manufacturing," Materials and Manufacturing Processes, vol. 35, no. 7, pp. 852-858, 2020.

[29] D. S. Nagesh and G. L. Datta, "Prediction of Weld Bead Geometry and Penetration in Shielded Metal-Arc Welding Using Artificial Neural Networks," Journal of Materials Processing Technology, vol. 123, no. 2, pp. 303-312, April 2002.

[30] S. Jindal, R. Chhibber, and N. P. Mehta, "Effect of Welding Parameters on Bead Profile, Microhardness and H2 Content in Submerged Arc Welding of High-Strength Low-Alloy Steel," Proceedings of the Institution of Mechanical Engineers, Part B: Journal of Engineering Manufacture, vol. 228, no. 1, pp. 82-94, January 2014.